Electrochemical study of asymmetric aqueous supercapacitors based on high density oxides: C/Ba0.5Sr0.5Co0.8Fe0.2O3-δ and FeWO4/Ba0.5Sr0.5Co0.8Fe0.2O3-δ

Pierre Lannelongue, Steven Le Vot, Olivier Fontaine, Thierry Brousse, Frédéric Favier

Electrochemical study of asymmetric aqueous supercapacitors based on high density oxides: C/$Ba_{0.5}Sr_{0.5}Co_{0.8}Fe_{0.2}O_{3-\delta}$ and $FeWO_4$/$Ba_{0.5}Sr_{0.5}Co_{0.8}Fe_{0.2}O_{3-\delta}$

Pierre Lannelongue[1,3], Steven Le Vot[1,3], Olivier Fontaine[1,3], Thierry Brousse[2,3] and Fréderic Favier[1,3,*]

[1] Institut Charles Gerhardt Montpellier (ICGM), UMR 5253, Université de Montpellier, CNRS, 34095 Montpellier Cedex 5, France

[2] Institut des Matériaux Jean Rouxel (IMN), UMR 6502, Université de Nantes, CNRS, 44322 Nantes Cedex 3, France

[3] Réseau sur le Stockage Electrochimique de l'énergie (RS2E), FR CNRS 3459, France

*frederic.favier@umontpellier.fr

Abstract

Two asymmetric aqueous electrochemical capacitors operated in 5M $LiNO_3$ are reported: C/$Ba_{0.5}Sr_{0.5}Co_{0.8}Fe_{0.2}O_{3-\delta}$ (BSCF) and $FeWO_4$/BSCF, with activated carbon and $FeWO_4$ (synthesized by a precipitation method) as negative electrodes, respectively, and BSCF (synthesized by a modified glycine-nitrate process) as positive electrodes. These two devices were operated between 0 and 1.6 V and between 0 and 1.4 V, respectively. They demonstrated a remarkable cycling ability with a high capacitance retention over 10,000 and 45,000 cycles, respectively. Thanks to the high density of BSCF, the C/BSCF device exhibits a volumetric energy density up to 2.7 $Wh.L^{-1}$ at low current densities. This study demonstrates the advantages and limits of the use of high density multicationic oxides with pseudocapacitive behavior to improve the volumetric energy density of aqueous electrochemical capacitors.

Keywords

Aqueous electrochemical capacitors; Supercapacitors; Asymmetric devices; Volumetric energy density; BSCF; $FeWO_4$; Perovskite.

1. Introduction

Electrochemical capacitors, also called supercapacitors, present intermediate performance between batteries and conventional capacitors [1]. Currently, commercialized electrochemical capacitors are electrochemical double layer capacitors (EDLCs) using activated carbon as electrodes. Their specific energy and power densities are about 10 $Wh.kg^{-1}$ [1] and 10 $kW.kg^{-1}$ [2], respectively. However, their volumetric energy density is low, typically between 5 and 7 $Wh.L^{-1}$. As such, EDLCs are not the ideal devices for power applications where the volume dedicated to energy storage is limited, such as in modern electrical terrestrial vehicles. Another type of electrochemical capacitors has been developed over the past two decades, using materials showing a pseudocapacitive behavior. The pseudocapacitive charge storage process induces a similar electrochemical signature to that of capacitive process, but its origin is faradic and involves fast and reversible redox reactions [1,3]. Such behavior has been observed for various electrode materials including metal oxides such as RuO_2 [4-6], MnO_2 [7-9], Fe_3O_4 [10,11], but also nitrides such as VN [12,13] and Mo_xN [14], conducting polymers [15] or Mxenes [16]. Thanks to their high density compared to that of activated carbon, pseudocapacitive oxides are attractive materials to improve the volumetric energy density of electrochemical capacitors. As such, Goubard-Bretesché et al. predicted a volumetric energy density of a symmetrical electrochemical capacitor MnO_2/MnO_2 (bulk density: 4.5 $g.cm^{-3}$) twice greater than that of a symmetrical carbon/carbon device (bulk density: 2.09-2.23 $g.cm^{-3}$) while keeping the same gravimetric specific energy [17].

Thus, high density pseudocapacitive oxides have to be considered to improve the volumetric energy density of electrochemical capacitors. This is in the last few years only that multicationic oxides have been studied as electrode materials for electrochemical capacitors [18]. Among them, ABO_3 perovskite materials [19-23], AB_2O_4 spinel materials [24-27], MWO_4 tungstate materials [28] or $A_2B_2O_7$ pyrochlore materials [29] have been considered. These materials present high densities but also specific capacitances close to that of standard activated carbon. In previous papers, some of us have reported the attractive properties of two oxides to be used as electrode materials for electrochemical capacitors: $FeWO_4$ [28] and $Ba_{0.5}Sr_{0.5}Co_{0.8}Fe_{0.2}O_{3-\delta}$, so called BSCF [30]. An asymmetric aqueous electrochemical capacitors with a $FeWO_4$ negative electrode material has already been tested using MnO_2 as the positive electrode [31]. This device presents a specific capacitance of 9 $F.g^{-1}$ (total weight of both electrodes) at 20 $mV.s^{-1}$ in 5M $LiNO_3$ with a high cycling ability over 40,000 cycles. The crystallographic density of $FeWO_4$ and BSCF materials is 7.5 and 5.8 $g.cm^{-3}$, respectively, *i.e.* 6 to 7 times greater than that of standard activated carbon. As such, both materials present high volumetric capacitance in aqueous medium (5M $LiNO_3$). Furthermore, their respective operational potential windows are complementary (-0.6 – 0 V *vs* Ag/AgCl for $FeWO_4$ and 0 – 0.8 V *vs* Ag/AgCl for BSCF). Thus, it seems interesting to evaluate the volumetric performance of such electrochemical capacitor devices built from these two electrode materials.

Electrochemical capacitor devices with BSCF positive electrodes have never been reported in the literature. As such, we report hereafter the study of two asymmetric devices: the first one associates an activated carbon electrode with a BSCF electrode (C/BSCF) and the second one associates $FeWO_4$ and BSCF electrodes ($FeWO_4$/BSCF). Both devices were operated in aqueous 5M $LiNO_3$ electrolyte. Several devices have been built and tested to determine the conditions, in terms of electrode weight ratios and current densities, allowing a good

compromise between performances and electrochemical stability window of each electrode. Specific and volumetric performance and cycling ability of these devices have been evaluated by galvanostatic cycling. Self-discharge measurements have been performed by a chronoamperometry/chronopotentiometry routine. Performance of these devices are commented to argue on the interest of using high density electrode materials to improve the volumetric energy density of electrochemical capacitors.

2. Experimental section

2.1. Materials

$Ba_{0.5}Sr_{0.5}Co_{0.8}Fe_{0.2}O_{3-\delta}$ – BSCF

All precursors were purchased from Sigma Aldrich. Precursors mass used are listed in **Tab.S1**. BSCF was prepared by a modified glycine-nitrate process. $Ba(NO_3)_2$ (ACS Reagent, ≥99%), $Sr(NO_3)_2$ (ACS Reagent, ≥99%), $Co(NO_3)_2$,$6H_2O$ (ACS Reagent, ≥98%) and $Fe(NO_3)_3$,$9H_2O$ (ACS Reagent, ≥98%) were dissolved in stoichiometric quantities in distilled water at 100°C and under vigorous stirring. A red solution is obtained. After dissolution, glycine (ACS Reagent, ≥98.5%), acting as complexing agent and fuel, was added to the solution. Ten minutes after glycine dissolution, ethylenediaminetetraacetique acid EDTA, acting as complexing agent (anhydrous, ≥99%) was added. The stoichiometry quantities of glycine and EDTA were determined following reactions pathways (1) and (2) respectively:

$$0.5\ Ba(NO_3)_2 + 0.5\ Sr(NO_3)_2 + 0.8\ Co(NO_3)_2 + 0.2\ Fe(NO_3)_3 + 2.13\ HOOC\text{-}CH_2\text{-}NH_2 \rightarrow Ba_{0.5}Sr_{0.5}Co_{0.8}Fe_{0.2}O_3 + 4.26\ CO_2 + 5.33\ H_2O + 3.165\ N_2 \quad (1)$$

$$0.5\ Ba(NO_3)_2 + 0.5\ Sr(NO_3)_2 + 0.8\ Co(NO_3)_2 + 0.2\ Fe(NO_3)_3 + 0.48\ C_{10}H_{16}N_2O_8 \rightarrow Ba_{0.5}Sr_{0.5}Co_{0.8}Fe_{0.2}O_3 + 4.8\ CO_2 + 3.84\ H_2O + 2.58\ N_2 \quad (2)$$

In order to synthesize large amounts of BSCF, expected glycine and EDTA masses were multiplied by 2.5 and 2, respectively. After EDTA dissolution, a 60 mL purple-black solution is obtained. At the end of the water evaporation (about one hour), the gelification process started. The gel was then transferred in an oven at 600°C under air atmosphere where a combustion took place 10 minutes later. Resulting ashes were kept at 600°C for one hour to remove carbon residues. Finally, ashes were manually ground and heated at 850°C for 10 hours.

$FeWO_4$

$FeWO_4$ was synthesized by a precipitation method. Two equimolar 15 mL solutions of $FeCl_2.4H_2O$ (puriss. p.a., ≥99%) and $Na_2WO_4.2H_2O$ (ACS Reagent, ≥99%), both from Sigma Aldrich were prepared. Precursor mass used are listed in **Tab.S2**. The iron chloride solution was heated at 70°C under magnetic stirring for 10 minutes. Then, the sodium tungstate was added dropwise into the iron chloride solution leading to a brow precipitate. The resulting solution was kept at 70°C under magnetic stirring for 3 hours. The precipitate was recovered by filtration before being washed three times with distilled water and subsequently three times with ethanol.

Activated carbon

Activated carbon was purchased from ACS Material®. The particle average size is 5 µm. Activated carbon from ACS Material® is mesoporous with a pore size distribution from 2 to 2.2 nm and its BET specific surface area is 2,000 $m^2.g^{-1}$.

2.2.BSCF and $FeWO_4$ powder characterizations

Prepared BSCF and $FeWO_4$ powders were characterized by X-ray diffraction using a PANalytical X'Pert in the Bragg-Brentano configuration with CuKα radiation, from 10 to 90° with a step angle of 0.032°. Their morphology were observed by scanning electron microscopy on a Hitachi S4800. BSCF composition was evaluated by EDS analysis.

2.3.Electrode preparation

Electrodes were prepared by mixing active materials with acetylene black (Alfa Aesar) and PTFE (60 wt% dispersed in water, Sigma Aldrich) in ethanol. Mass ratios (active material: acetylene black: PTFE) were 60:30:10 for BSCF and $FeWO_4$ based electrodes and 75:15:10 for activated carbon based electrodes. After ethanol evaporation at 60°C under magnetic stirring, the resulting paste was repeatedly cold rolled until a homogeneous film was obtained. A 10 mm diameter disk was cut off from the film and pressed at 10 tons onto a folded stainless steel grid. For asymmetric devices (Swagelok type), electrode films were pressed onto nickel foam at 10 tons. Then, a 6 mm diameter disk shape was cut off. Electrode loadings used for electrochemical tests were 3.2-4.0 $mg_{carbone}.cm^{-2}$ (5.3-6.7 $mg_{electrode}.cm^{-2}$), 4.4-15.3 $mg_{BSCF}.cm^{-2}$ (7.4-25.5 $mg_{electrode}.cm^{-2}$) and 4.7-5.5 $mg_{FeWO4}.cm^{-2}$ (7.8-9.2 $mg_{electrode}.cm^{-2}$).

In contrast with the 20 wt% usually used, a larger amount of acetylene black was necessary to fabricate BSCF and $FeWO_4$ electrodes. Only from 30 wt%, a percolation threshold was reached allowing electrodes to have a sufficient electronic conductivity for optimal performances. At lower acetylene black content, the electrochemical signature of electrodes was less capacitive and a specific capacitance twice lower was obtained **[30]**. Furthermore, the specific capacitance of acetylene black in these electrodes is 1 $F.g^{-1}$. With respect to the measured electrode capacitances such limited contribution was neglected.

2.4.Electrochemical tests

BSCF, $FeWO_4$ and activated carbon -based electrodes were first tested in a three electrode cell with a platinum counter electrode and an Ag/AgCl reference electrode. Cyclic voltammetry was performed in 5M $LiNO_3$ at 5 $mV.s^{-1}$ to determine their potential window and specific capacitance. Specific capacitances $C_{spe,electrode}$ (in $F.g^{-1}$) are calculated with the following equation:

$$C_{spe,electrode} = \frac{\int_{V_i}^{V_f} i.dV}{\Delta V.\upsilon.m} \quad (3)$$

With $\int_{V_i}^{V_f} i.dV$ the voltammogramm positive part area (in A.s), ΔV the potential window (in V), υ the scan rate (in $V.s^{-1}$) and m the active material mass (in g).

Asymmetric C/BSCF and $FeWO_4$/BSCF device specific and volumetric performance were evaluated by cyclic voltammetry and galvanostatic cycling (in a current density range from 0.2 to 4 $A.g^{-1}$ of active material in both electrodes) in a three electrode Swagelok cell with an Ag/AgCl reference electrode, in aqueous 5M $LiNO_3$. Both electrodes were separated with glass microfibers separators (Wathman® paper). By cyclic voltammetry, the device capacitances C (in F), specific capacitances C_{spe} (in $F.g^{-1}$) and volumetric capacitances C_{vol} (in $F.cm^{-3}$) were calculated using equations 4, 5 and 6 respectively.

$$C = \frac{\int_{V_i}^{V_f} i.dV}{\Delta U.\upsilon} \quad (4)$$

$$C_{spe} = \frac{C}{m'} \quad (5)$$

$$C_{vol} = \frac{C}{V} \quad (6)$$

Where ΔU is the device cell voltage, in V, m' is the active material mass in both electrodes in g and V is the geometrical volume of both electrodes and the geometrical volume of both nickel foam current collectors in cm^3.

The capacitance C, the maximum energy E_{max} (in Wh) and power densities P_{max} (in W) were calculated from galvanostatic cycling and with equations 7, 8 and 9:

$$C = i.\frac{\int_{t_i}^{t_f} \Delta U.dt}{\Delta U^2} \quad (7)$$

$$E_{max} = \frac{1}{2}.C.\Delta U^2 \quad (8)$$

$$P_{max} = \frac{\Delta U^2}{4.R} \quad (9)$$

Where i is the applied current density, ΔU is the cell voltage of the device of the device and R is the equivalent series resistance (Ω) obtained by ohmic drop measurement during galvanostatic cycling. Specific performance (and specific capacitances) were calculated by taking into account the active material mass of both electrodes (Eq. 5). As the specific capacitance of acetylene black used in the electrodes is less than 1 $F.g^{-1}$, its contribution was neglected. Volumetric performance were obtained by taking into account both electrodes and nickel foam current collector volume (Eq. 6). Self-discharge behaviors were evaluated

through chronopotentiometry technique. Before this step, devices were fully galvanostatically charged and the cell were kept at their maximum cell voltage during 3 hours before letting the device self-discharged. Cycling ability of C/BSCF and $FeWO_4$/BSCF devices was evaluated by galvanostatic cycling. All electrochemical tests were performed using a VMP3 potentiostat-galvanostat from Biologic running with the EC-Lab software. A 5M $LiNO_3$ electrolyte was used as the best specific capacitances for both BSCF and $FeWO_4$ electrodes were obtained in this given electrolyte.

3. Results and discussion

3.1.BSCF and $FeWO_4$ powder characterizations

BSCF and $FeWO_4$ XRD patterns are shown in **Fig. S1**. BSCF XRD pattern is characteristic of a perovskite structure with the expected Pm-3m space group. BSCF XRD pattern is similar to those of previous studies where BSCF was prepared by various sol-gel synthesis **[32-36]**, including the glycine-nitrate process **[32]**, and by solid state reaction **[35]**, which all needed a minimum calcination temperature of 900°C. $FeWO_4$ XRD pattern shows broad peaks of low intensities, characteristic of the poor crystallinity of $FeWO_4$ prepared by precipitation method. $FeWO_4$ XRD pattern is different of those of $FeWO_4$ prepared by hydrothermal synthesis of polyol-mediated synthesis which allowed to prepare crystalline particles because a minimum annealed temperature of 180°C was used **[28,37]**. In our case, the temperature used from the beginning to the end of the synthesis is 70°C and the XRD pattern is similar to the one of $NiWO_4$ prepared by the same route **[38]**. EDS analysis of BSCF powder showed that the atomic ratio Ba/Sr is close to 1. Furthermore, the atomic percentage of Co in the B site of the perovskite is 80%. Finally, the atomic ratio (Ba+Sr)/(Co+Fe) is close to 1 (see **Tab. S3**). The overall chemical composition is thus confirmed for the prepared BSCF. SEM pictures of

BSCF and $FeWO_4$ powders are depicted in **Fig. S2**. BSCF prepared powder is composed of 5-20 µm particles whereas $FeWO_4$ SEM micrography shows that the powder is composed of 20-40 nm particles.

3.2.Electrochemical tests with BSCF, $FeWO_4$ and activated carbon electrodes

In **Fig. 1** are shown the cyclic voltammograms (CVs) of BSCF (50^{th} cycle), $FeWO_4$ (10^{th} cycle) and activated carbon (10^{th} cycle) based electrodes, recorded in 5M $LiNO_3$ at 5 $mV.s^{-1}$. BSCF CV (**Fig. 1a**) depicts a box-type shape characteristic of a material with a pseudocapacitive behavior, with some distortions from the typical rectangular shape. BSCF - based electrode is stable from 0 to 0.8 V *vs* Ag/AgCl and displays a specific capacitance of 57 $F.g^{-1}$ (46 $C.g^{-1}$). As such, it can be used as positive electrode material. Above 0.8 and below 0 V *vs* Ag/AgCl, the current increases (in absolute value). This is assigned to oxygen and hydrogen evolution reactions, respectively. In the present case, the 50^{th} cycle is the cycle from which the CV shape and the specific capacitance does not change anymore. From the 1^{st} to the 50^{th} cycle, an increase of the specific capacitance from 30 to 57 $F.g^{-1}$ was observed. $FeWO_4$ has already been studied as negative electrode material for supercapacitors. The electrode made from $FeWO_4$ prepared by a precipitation method is stable from -0.6 to 0V *vs* Ag/AgCl (**Fig. 1b**) and displays a specific capacitance of 60 $F.g^{-1}$ (36 $C.g^{-1}$). Stable CV shape of $FeWO_4$ were rapidly obtained (10 cycles). From the 1^{st} cycle to the 10^{th}, only a very slight change in specific capacitance was observed. The charge storage mechanism in $FeWO_4$ electrode involves the Fe^{2+}/Fe^{3+} redox couple. Potential below -0.7 V *vs* Ag/AgCl should be avoided because Fe^{2+} is irreversibly reduced to Fe^0. CV of activated carbon (as negative electrode) is representative of a capacitive behavior (**Fig. 1c**). This electrode can be cycled from -0.8 to 0 V *vs* Ag/AgCl. Below -0.8 V *vs* Ag/AgCl, the current increases (in absolute

value), which suggests that the hydrogen evolution reaction begins, causing electrolyte degradation. In this potential window, its specific capacitance is 160 $F.g^{-1}$ (128 $C.g^{-1}$) at 5 $mV.s^{-1}$. According to these tests, two types of asymmetric devices can be built. The first one, C/BSCF, is designed by associating a negative electrode made of activated carbon and a BSCF positive electrode. The second one is an all oxide device, with a negative electrode made of $FeWO_4$ and a BSCF positive electrode.

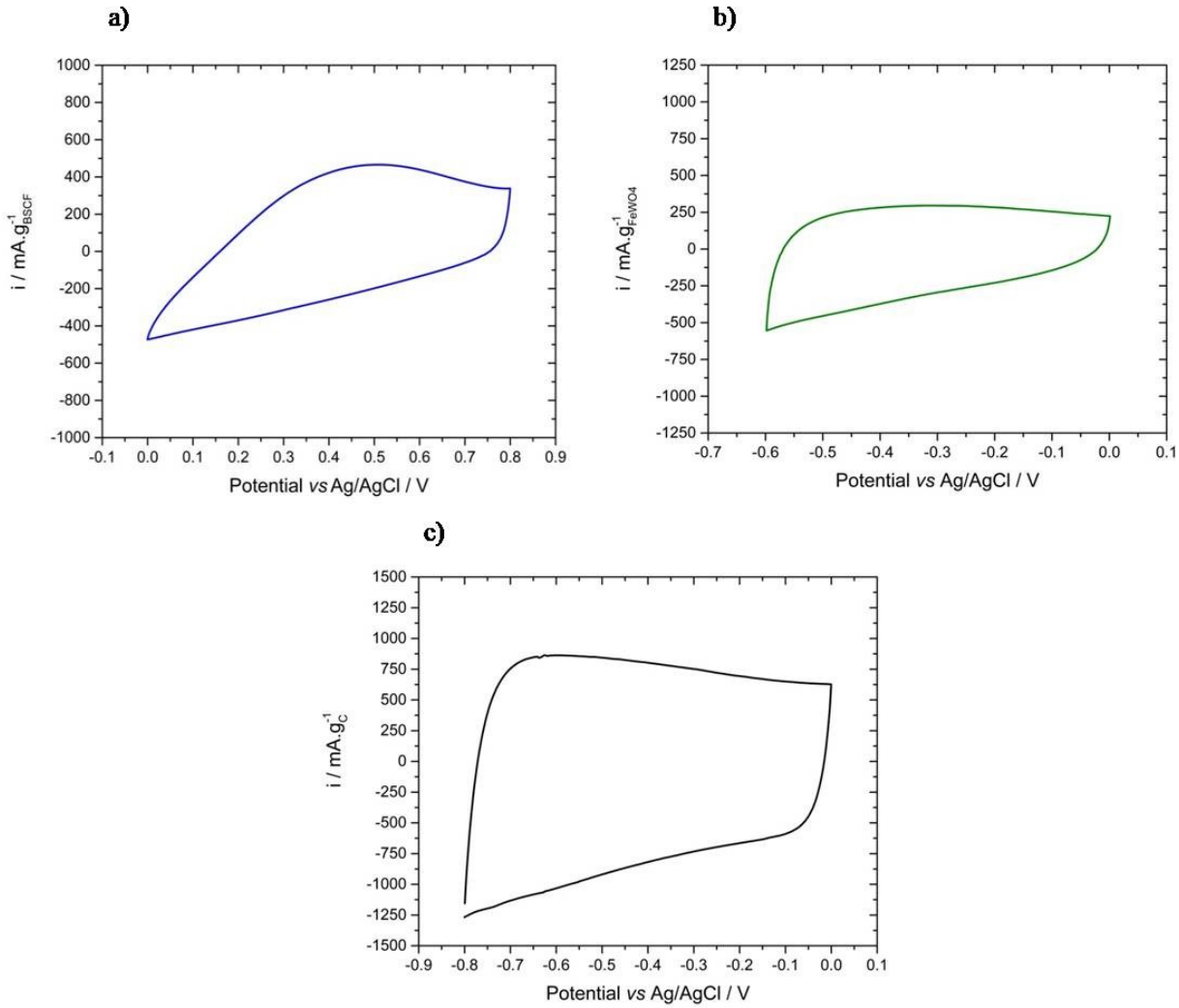

Fig. 1.CVs recorded at 5 $mV.s^{-1}$ in aqueous 5M $LiNO_3$ of a) BSCF based electrode (50^{th} cycle), b) $FeWO_4$ based electrode (10^{th} cycle) and c) activated carbon electrode (10^{th} cycle); gravimetric values are expressed per active weight in electrodes.

3.3. Asymmetric devices

To keep electrode cycling in their respective potential windows, charge balance of the device has to be ensured by using an accurate weight ratio of active materials in both electrodes (calculated by taking into account electrode capacities and potential windows) [39]. However, since each electrode material has different capabilities upon scan rate (or current density), this weight ratio can only be determined for a given scan rate or a given current density. In the next section, the methodology was as followed. Firstly, weight ratios were calculated to design asymmetric devices with the aim to be cycled at 5 $mV.s^{-1}$ (or corresponding current density) in 5M $LiNO_3$ electrolyte. These specific ratios were determined using equation (10):

$$\frac{m^{+}}{m^{-}} = \frac{C^{-}}{C^{+}} \qquad (10)$$

Where m^+ and m^- are the active material mass in the positive and the negative electrode respectively and C^+ and C^- are the capacities (in $C.g^{-1}$) of the positive and negative electrode respectively.

After analysis of the results (capacitances and electrochemical stability windows of electrodes), several devices with various electrode weight ratios were designed and tested by galvanostatic cycling at various current densities with the aim to find the optimal conditions allowing a good compromise between the device performances and the electrochemical stability windows of each electrodes. In this section, from one weight ratio to another, performances are not compared at the same current density, but in conditions electrodes cycle in their respective electrochemical stability window (*i.e.* in conditions a fast degradation of the device, caused by water splitting, is avoided). The conditions, in terms of electrode weight

ratios and current densities, leading to the best compromise between electrochemical stability of electrodes and performances, were used to test the longterm cycling ability and self-discharge behavior of the fabricated asymmetric devices.

3.3.1. Asymmetric C/BSCF devices

As mentioned in paragraph 3.2., specific capacities of BSCF and activated carbon (as negative electrode) in 5M $LiNO_3$ at 5 $mV.s^{-1}$ are 46 and 128 $C.g^{-1}$, respectively. Thus, a theoretical BSCF/C weight ratio of 2.8 is expected to allow the electrodes to cycle in their respective stable potential windows (*i.e.* from 0 to 0.8 V *vs* Ag/AgCl for BSCF and from -0.8 to 0 V *vs* Ag/AgCl for activated carbon). As such, electrode loadings used to build this device with a BSCF/C weight ratio of 2.8 were 14.2 $mg_{BSCF}.cm^{-2}$ and 5.0 $mg_{C}.cm^{-2}$.

Fig. S3 depicts C/BSCF CV from 0 to 1.6 V (according to the electrochemical window of each electrodes), together with those of activated carbon and BSCF electrodes. The CV shape of the full device is rectangular as expected for an electrochemical capacitor. However, as shown in **Fig. S3**, activated carbon and BSCF do not cycle in their respective electrochemical window. In such a case, potential windows of activated carbon and BSCF based electrodes are -1.0 – -0.1 V *vs* Ag/AgCl and -0.1 – 0.6 V *vs* Ag/AgCl, respectively. As mentioned above, at -1.0 V *vs* Ag/AgCl, water is reduced at the carbon electrode surface and loss of performance upon cycling the cell is likely to occur because of this electrolyte degradation. Actually, the same shift in the electrode potential windows was observed when using a current density ranging from 0.1 to 4 $A.g^{-1}$ (of active material). As such, the BSCF/C weight ratio of 2.8 was no longer considered for the rest of the study.

To evaluate C/BSCF performance, several devices with various BSCF/C weight ratio have then been prepared and tested. BSCF/C weight ratio were 1.5, 2.1, 2.4 and 3.6. CVs at 5 $mV.s^{-}$

[1] of the fabricated devices are reported in **Fig. S4**. Total mass of active material and total volume of electrodes and current collectors used to evaluate device performance are listed in **Tab. S4** together with the capacitances and the specific capacitances. Despite a slight decrease for the weight ratio of 3.6, the greater the weight ratio, the greater the measured capacitance. In contrast, the greater electrode masses needed for the highest weight ratio strongly impacted on the corresponding specific capacitances, as the greater the weight ratio, the lower the specific capacitance. Looking closer at electrode CVs in **Fig. S4**, one can notice that electrodes were operated in their safe electrochemical window only for the device with a weight ratio of 1.5, *i.e.* between 0 and -0.8 V *vs* Ag/AgCl for activated carbon electrode and between 0 and +0.8 V *vs* Ag/AgCl for BSCF electrode. For the other devices, the activated carbon electrode potential window decreases down to -0.8 V *vs* Ag/AgCl (hence, BSCF electrode potential window does not reach + 0.8 V *vs* Ag/AgCl) which could lead to electrolyte degradation.

Energy and power densities of these devices have been determined from galvanostatic cycling by applying current densities ranging from 0.2 to 4 $A.g^{-1}$ (total mass of active materials in the cell). Specific and volumetric performance are shown in **Fig. 2a and 2b**, respectively, as well as the Ragone plots. The corresponding galvanostatic cycles are depicted in **Fig. S5**. As generally observed for electrochemical capacitors, the energy density of fabricated C/BSCF devices decreased as the applied current density increased. At low current density, *i.e.* 0.2 $A.g^{-1}$, the greater the BSCF/C weight ratio, the lower the energy and the power densities (both specific and volumetric). This behavior was assigned to both lower capacitances and greater electrode masses and volumes as the BSCF/C weight ratio increased. At 0.2 $A.g^{-1}$, the C/BSCF device with a weight ratio of 1.5 presented the greatest energy densities in the series at 8.6 $Wh.kg^{-1}$ and 2.7 $Wh.L^{-1}$. A similar trend was observed for power densities. At 0.2 $A.g^{-1}$, power densities ranged from 5.6 to 3 $kW.kg^{-1}$ and from 1.8 to 1.4 $kW.L^{-1}$, depending on the

BSCF/C weight ratio. With the increase of the current density at 4 $A.g^{-1}$, the C/BSCF device with a weight ratio of 2.1 showed the greatest energy densities with 3.7 $Wh.kg^{-1}$ and 1.3 $Wh.L^{-1}$. Compared to the device with a 1.5 weight ratio, this energy density improvement originated from a greater capacitance (37 mF for a ratio of 2.1 *vs* 27 mF for a ratio of 1.5) which allowed to compensate for the larger mass and volume of the electrodes. However, power densities at the highest current density followed the same trend as 0.2 $A.g^{-1}$. Power

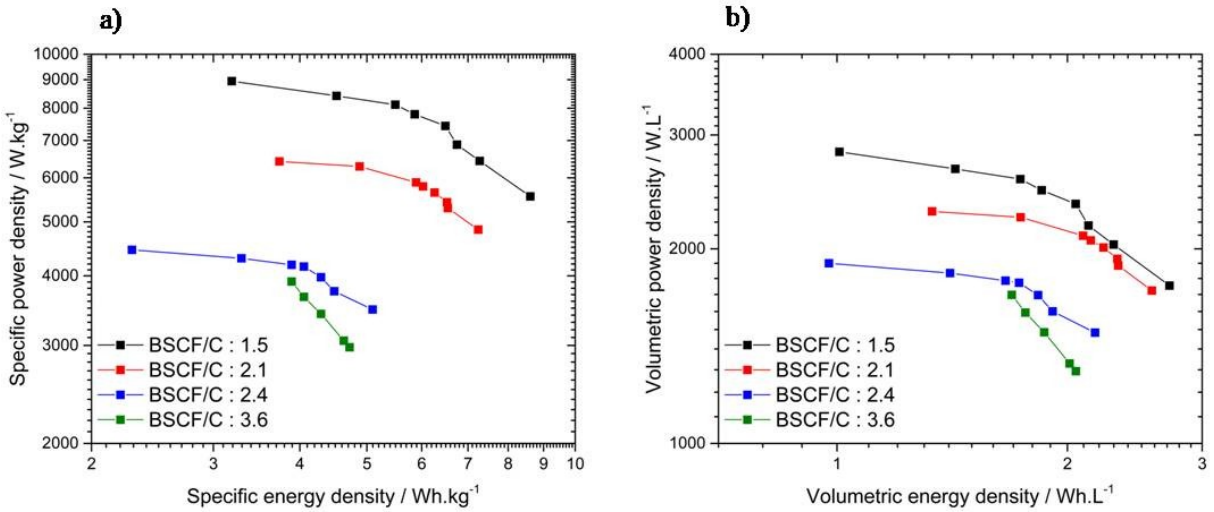

densities decreased from 8.9 to 4.4 $Wh.kg^{-1}$ and from 2.8 to 1.9 $Wh.L^{-1}$ when the weight ratio increases.

Fig. 2. Ragone plots representing the evolution of the power density *vs* the energy density of the four C/BSCF devices tested in 5M $LiNO_3$ with BSCF/C ratios of 1.5 (black), 2.1 (red), 2.4 (blue) and 3.6 (green). Current densities applied are 0.2, 0.5, 0.6, 0.8, 1.0, 1.2, 2.0 and 4 $A.g^{-1}$. Graph a) specific power and energy densities and b) volumetric power and energy densities; gravimetric values are expressed per total active weights in both electrodes and volumetric values per volume of both electrodes and their current collector. Calculations have been done using Eqs (9) and (10).

In the whole range of applied current densities, only a single current density applied for each C/BSCF device allows to operate BSCF and C electrodes in their safe electrochemical window. These are 0.2, 0.5, 0.5 and 1.2 $A.g^{-1}$ for C/BSCF devices with weight ratio of 1.5, 2.1, 2.4 and 3.6, respectively. Respective galvanostatic cycles at such current densities are shown in **Fig. S6** and corresponding performance are reported in **Tab. 1**. Potential ranges of

activated carbon and BSCF electrodes at such optimized current densities are -0.8 – 0 V *vs* Ag/AgCl and 0 – 0.8 V *vs* Ag/AgCl, respectively, corresponding to targeted electrochemical stability windows of both electrodes. For lower current densities, activated carbon electrode potential goes below -0.8 V *vs* Ag/AgCl and for higher current densities, BSCF electrode potential rises to 0.8 V *vs* Ag/AgCl and above. According to **Tab. 1**, increasing the BSCF/C weight ratio allows to reach greater charge and discharge rates. To fabricate the most performing C/BSCF device, a BSCF/C weight ratio of 1.5 and a 0.2 $A.g^{-1}$ current density should be considered. However, in these conditions, a large discrepancy between charge and discharge times is observed. To avoid this unbalanced characteristic, the device with a weight ratio of 2.1 operated at a current density of 0.5 $A.g^{-1}$ was selected for further tests. To move a step forward in the device characterization, self-discharge measurements and cycling ability tests were performed on a C/BSCF device with a weight ratio of 2.1 at 0.5 $A.g^{-1}$, and are presented in section 3.3.3.

Tab. 1. Specific energy and power densities (E_{spe} and P_{spe}), volumetric energy and power densities (E_{vol} and P_{vol}) of C/BSCF full devices with BSCF/C weight ratio of 1.5, 2.1, 2.4 and 3.6 recorded in 5M $LiNO_3$ at 0.2, 0.5, 0.5 and 1.2 $A.g^{-1}$, respectively; gravimetric values are expressed per total active weights in both electrodes and volumetric values per volume of both electrodes and their current collector.

BSCF/C Weight ratio	**E_{spe} $Wh.kg^{-1}$**	**P_{spe} $kW.kg^{-1}$**	**E_{vol} $Wh.L^{-1}$**	**P_{vol} $kW.L^{-1}$**
1.5	8.6	5.5	2.7	1.7
2.1	6.5	5.3	2.3	1.9
2.4	4.5	3.8	1.9	1.6
3.6	3.9	3.9	1.8	1.8

3.3.2. Asymmetric $FeWO_4$/BSCF devices

The study on all oxide asymmetric $FeWO_4$/BSCF devices followed the same methodology as for C/BSCF devices. According to specific capacities measured for $FeWO_4$ and BSCF electrodes, respectively 36 and 46 $C.g^{-1}$ at 5 $mV.s^{-1}$ in 5M $LiNO_3$, a $FeWO_4$/BSCF weight ratio of 0.8 should lead to suitable potential windows for both electrodes. Alternatively, two other devices with $FeWO_4$/BSCF weight ratio at 1.67 and 2 were tested. These devices have been cycled between 0 and 1.4 V.

CVs of the various $FeWO_4$/BSCF device, together with those of their electrodes, are shown in **Fig. 3**. Total active material mass, total volume of electrodes and current collectors, capacitances and specific capacitances of fabricated devices are listed in **Tab. S5**. As for C/BSCF devices, the CV of $FeWO_4$/BSCF device shows a distorted rectangular shape, characteristic of a pseudocapacitive behavior. From $FeWO_4$/BSCF weight ratio at 0.8 to 2, specific capacitances are found to remain the same, close to 16-17 $F.g^{-1}$. The potential window of BSCF electrode, ranging approximately from 0 – 0.7 V *vs* Ag/AgCl, was fitting in its electrochemical stability window (0 – 0.8 V *vs* Ag/AgCl). However, the potential window of $FeWO_4$ electrodes ranged approximately from -0.7 – 0 V *vs* Ag/AgCl. This potential window could result in a fade of performance upon cycling since, at the lowest limit, the electrode potential is very close to that of the irreversible $Fe^{2+} \rightarrow Fe^0$ reduction reaction.

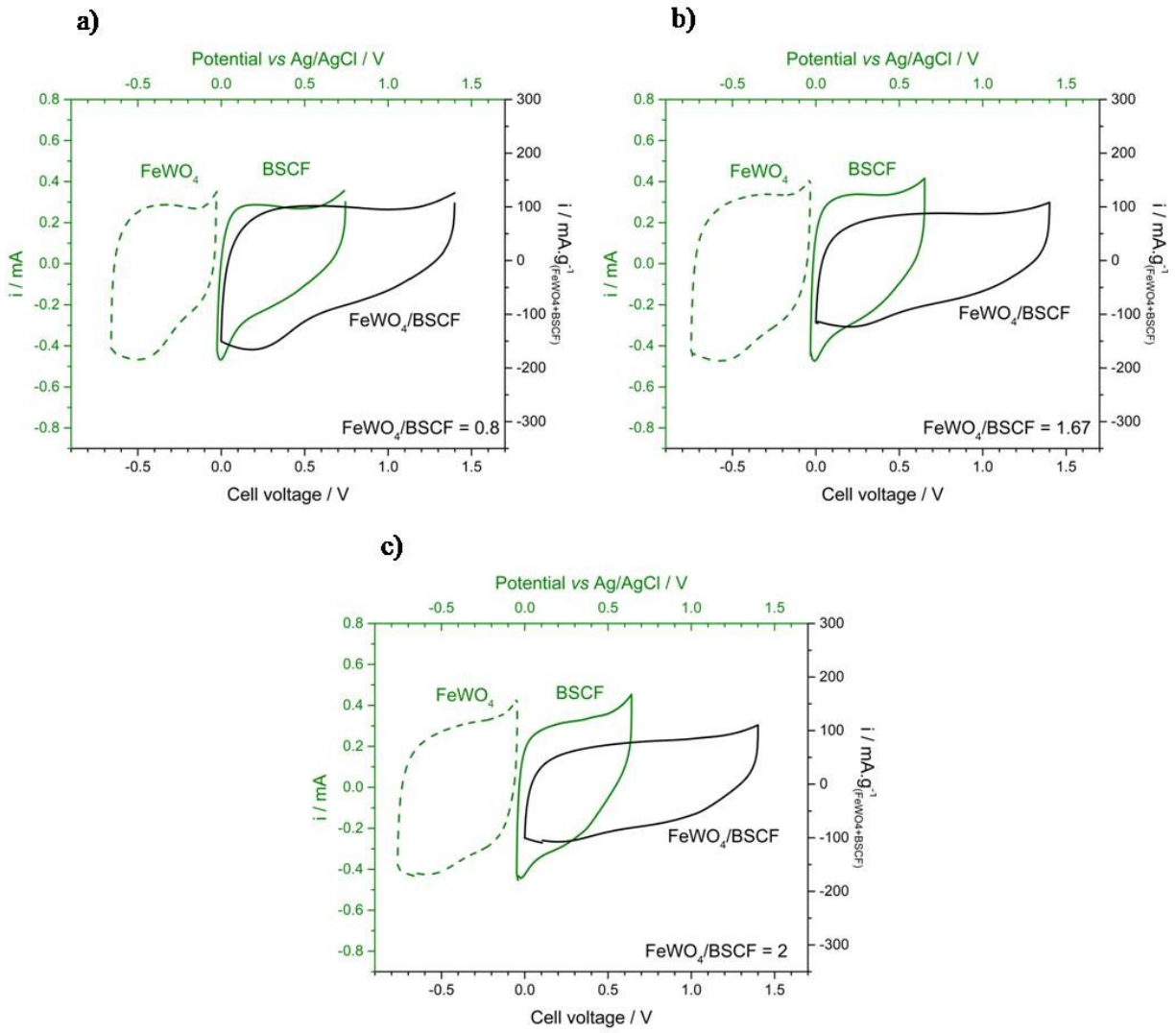

Fig. 3.CVs recorded at 5 $mV.s^{-1}$ in 5M $LiNO_3$ of $FeWO_4$/BSCF devices (black line) together with $FeWO_4$ (green dots) and BSCF electrodes (green line) CVs with BSCF/$FeWO_4$ weight ratio of a) 0.8, b) 1.67 and c) 2; gravimetric values are expressed per active weight in both electrodes.

To optimize the operating conditions for $FeWO_4$/BSCF devices and to evaluate their performance, galvanostatic cycling was performed at various current densities from 0.25 to 4 $A.g^{-1}$. Specific and volumetric densities are reported in **Fig. 4** and the galvanostatic cycles are depicted in **Fig. S7**. Performance of the $FeWO_4$/BSCF device with a weight ratio of 0.8 are not reported because, whatever the applied current density, the $FeWO_4$ electrode potential always reached potentials below -0.7 V *vs* Ag/AgCl. As such, poor coulombic efficiencies at 42 (at 0.25 $A.g^{-1}$) and 92 %(at 4 $A.g^{-1}$) were obtained, demonstrating the limited reversibility

of charge and discharge processes that could originate from an irreversible reduction of Fe^{2+} to Fe^{0}. As for C/BSCF devices, when the current density was greater, the corresponding energy density of $FeWO_4$/BSCF devices decreased, either with $FeWO_4$/BSCF weight ratio at 1.67 or 2. Specific and volumetric performance of the tested $FeWO_4$/BSCF devices were approximately the same but energy densities of the device with a weight ratio of 2 were slightly weaker. At 0.25 $A.g^{-1}$, energy densities of $FeWO_4$/BSCF devices with a ratio of 1.67 and 2 were 2.9 and 2.7 $Wh.kg^{-1}$ respectively, and 1.2 and 1.1 $Wh.L^{-1}$ respectively. At the same current density, power densities for both devices were similar at about 3.8 $kW.kg^{-1}$ and 1.5 $kW.L^{-1}$. When the current density is increased to 4 $A.g^{-1}$, energy densities of the devices with a ratio of 1.67 and 2 decreased to 1.1 and 1.0 $Wh.kg^{-1}$, respectively and to 0.5 and 0.4 $Wh.L^{-1}$, respectively. With these asymmetric devices, the limit of the $FeWO_4$ electrode potential window was lower than the expected value at -0.6 V *vs* Ag/AgCl. For each devices, a single current density allowed to limit the $FeWO_4$ electrode potential above -0.7 V *vs* Ag/AgCl, thus limiting the Fe^{2+} reduction to Fe^{0}. These current densities are 0.4 and 0.25 $A.g^{-1}$ of active material for $FeWO_4$/BSCF devices with weight ratio of 1.67 and 2, respectively (corresponding galvanostatic cycles are in **Fig. S8**). At such current densities, the devices showed the same energy densities of 2.7 $Wh.kg^{-1}$ and 1.1 $Wh.L^{-1}$. The $FeWO_4$/BSCF cycling ability and self-discharge behavior were further evaluated on the device with a $FeWO_4$/BSCF weight ratio of 2 operated at 0.25 $A.g^{-1}$.

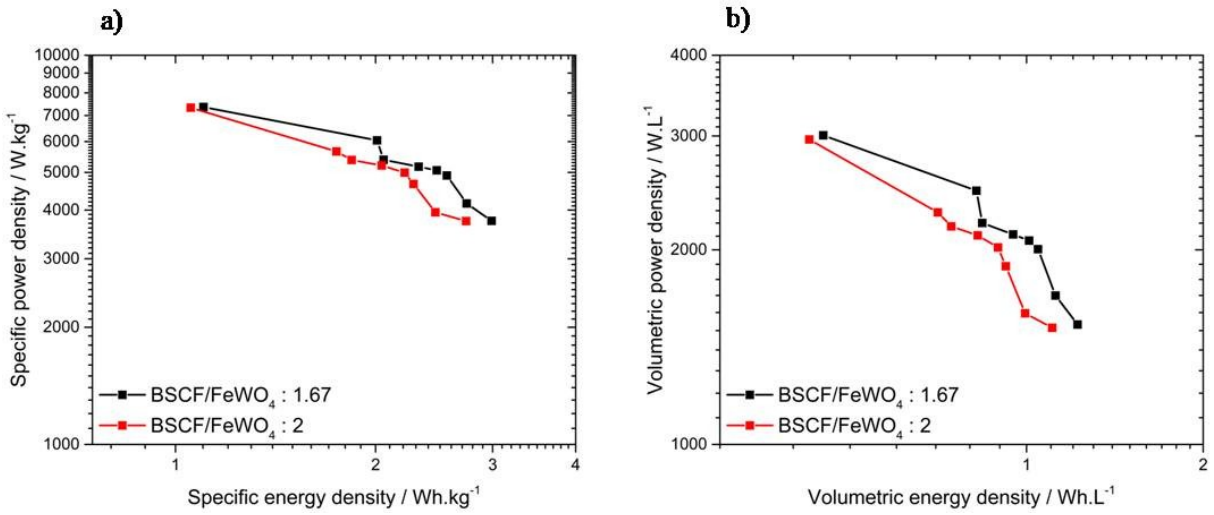

Fig. 4. Ragone plots representing the evolution of the power density *vs* the energy density of the two $FeWO_4$/BSCF devices tested in 5M $LiNO_3$ with BSCF/$FeWO_4$ ratio of 1.67 (black) and 2 (red). Current densities applied are 0.25, 0.4, 0.5, 0.6, 0.8, 1, 1.2 and 4 $A.g^{-1}$. Graph a) represents specific power and energy densities and b) represents volumetric power and energy densities; gravimetric values are expressed per total active weights in both electrodes and volumetric values per volume of both electrodes and their current collector. Calculations have been done using Eqs (9) and (10).

3.3.3. Cycling ability and self-discharge behavior of C/BSCF and $FeWO_4$/BSCF asymmetric devices

Cycling ability of C/BSCF (BSCF/C weight ratio of 2.1) and $FeWO_4$/BSCF ($FeWO_4$/BSCF weight ratio of 2) devices were evaluated in 5M $LiNO_3$ at 0.5 and 0.25 $A.g^{-1}$, respectively. The current densities were chosen according to balance the potential window of their electrodes. Evolutions of the specific capacitance of these devices *vs* number of cycles are depicted in **Fig. 5**. The specific capacitance of the C/BSCF device was 17 $F.g^{-1}$ at the beginning of the cycling test, as shown in **Fig. 5a**. First, the specific capacitance increases which is due to BSCF electrode activation. Then, it progressively decreased down to 15 $F.g^{-1}$ for the 10,000th cycle for an overall 12 % fading. This capacitance fading of the device could be due to the BSCF electrode behavior, as it showed a specific capacitance fading of approximately 10% over 2,000 cycles **[30]**, whereas activated carbon electrodes are known to be stable over

hundred thousands of cycles, eventually. Furthermore, coulombic efficiency of the device was above 98 % over the entire cycling test, demonstrating the good charge/discharge reversibility of the device. To go further, impedance spectroscopy was performed after the 10^{th} and the last cycle of the long term cycling test. Corresponding Nyquist diagrams are shown in **Fig. S9a**. The resistance measured at high frequencies, at the intercept between the EIS plot and the Z' axis, corresponds to the resistance of the separators impregnated by the electrolyte. This resistance is approximately 1 Ω after the 10^{th} cycle and does not seem to further increase after the $10{,}000^{th}$ cycle. At lower frequencies a semi-circle can be observed. It is usually assigned to the interface resistance between the active material and current collector **[40]**. This charge transfer resistance (0.8 Ω) showed limited changes upon cycling. It only increased up to 1 Ω from the 10^{th} to the $10{,}000^{th}$ cycle. The equivalent series resistance evaluated at high frequency was 2.7 Ω after 10 cycles and increased at 3 Ω after 10,000 cycles. The limited changes upon cycling of the various resistances measured demonstrate the high stability of the device.

Cycling ability of the $FeWO_4$/BSCF device has been evaluated over 45,000 cycles. The choice to apply for a greater number of cycles for this specific device was motivated by the opportunity to evaluate the cycling ability of an all-oxide device as only a few studies depict such performance over such a large number of cycles. Changes in the specific capacitance of the $FeWO_4$/BSCF device upon charge/discharge cycling at 0.25 $A.g^{-1}$ is shown in **Fig. 5b**. Its initial specific capacitance at 12 $F.g^{-1}$ goes down to 10 $F.g^{-1}$ at the end of the cycling test, corresponding to an overall 17% fading of the specific capacitance after 45,000 cycles. In comparison with the C/BSCF device, operated at 0.5 $A.g^{-1}$, the specific capacitance fading of the $FeWO_4$/BSCF device is limited to about 3% after the $10{,}000^{th}$ cycle, demonstrating the remarkable cycling ability of this device, especially when operated at a moderate current density of 0.25 $A.g^{-1}$. As it can be observed on this graph, the capacitance fading is more

pronounced after 22,000 cycles. This behavior is not necessarily assigned to the electrodes but to a non-optimized setup. The Coulombic efficiency of this device upon the entire cycling test is about 95%, lower than for C/BSCF or what is generally observed in electrochemical capacitors (98-99%). This can be due to some parasitic Fe^{2+} reduction reaction to Fe^0 because of a potential limit of $FeWO_4$ electrode close to -0.7 V *vs* Ag/AgCl. Nyquist diagrams after 10 cycles and 45,000 cycles are depicted in **Fig. S9b**. The resistance measured at high frequencies increased from 1.3 to 1.7 Ω after the 45,000th cycle. The semi-circle assigned to the charge transfer resistance is not clearly defined after 45,000 cycles, but, it is clear that this resistance was increased upon cycling. Finally, the equivalent series resistance also increased during cycling, from 7.4 to 18.3 Ω.

In the literature, only a few studies deal with long term stability evaluation of symmetric or asymmetric aqueous devices with at least one pseudocapacitive oxide. Among them, asymmetric devices were reported with a negative activated carbon electrode such as C/$BiMn_2O_5$ [41] and C/MnO_2 [42]. The first one presented only a 90% retention of its capacitance over 1,000 cycles (10 mA.cm^{-2}, 1.8 V, 0.5M Na_2SO_4). On the other hand, the C/MnO_2 device presented the greatest cycling ability ever reported in the literature with a 87.5% of retention over 195,000 cycles (40 mA.cm^{-2}, 2 V, 0.1M K_2SO_4). Some symmetric devices have also been tested, such as $ZnFe_2O_4$/$ZnFe_2O_4$ (composite electrodes with carbon nanotubes) which maintained only 70 % of its capacitance over 2,000 cycles (0.9 V, 1M LiCl) [43]. Finally, a few studies on asymmetric devices free of activated carbon have been reported. For example, VN/MnO_2 (composite electrodes with carbon nanotubes) retained only 80% of its initial capacitance over 1,000 cycles (10 mA, 1.8 V, 0.5M Na_2SO_4) [44]. The first asymmetric device with two oxides ever reported, Fe_3O_4/MnO_2, presented also a limited cycling ability with a 50% capacitance fading over 5,000 cycles (1.8 V, 0.1M K_2SO_4) [45]. As a comparison with this latter device, $FeWO_4$/MnO_2 device had a 84% retention over 40,000

cycles (20 mV.s^{-1}, 1.6 V, 5M $LiNO_3$) [31]. As MnO_2 electrode has demonstrated a fair cycling stability, the greater cycling ability of the $FeWO_4/MnO_2$ device when compared to that of Fe_3O_4/MnO_2 device was assigned to the stability of the Fe^{2+}/Fe^{3+} redox couple in the $FeWO_4$ structure. Initial C/BSCF device capacitance faded down by 12% over 10,000 cycles (0.5 A.g^{-1}, 1.6 V, 5M $LiNO_3$) while it was 17% fading for the $FeWO_4$/BSCF device over 45,000 cycles (0.25 A.g^{-1}, 1.4 V, 5M $LiNO_3$). This cycling ability, similar to that of $FeWO_4/MnO_2$, originates from the good cycling stability of individual electrodes.

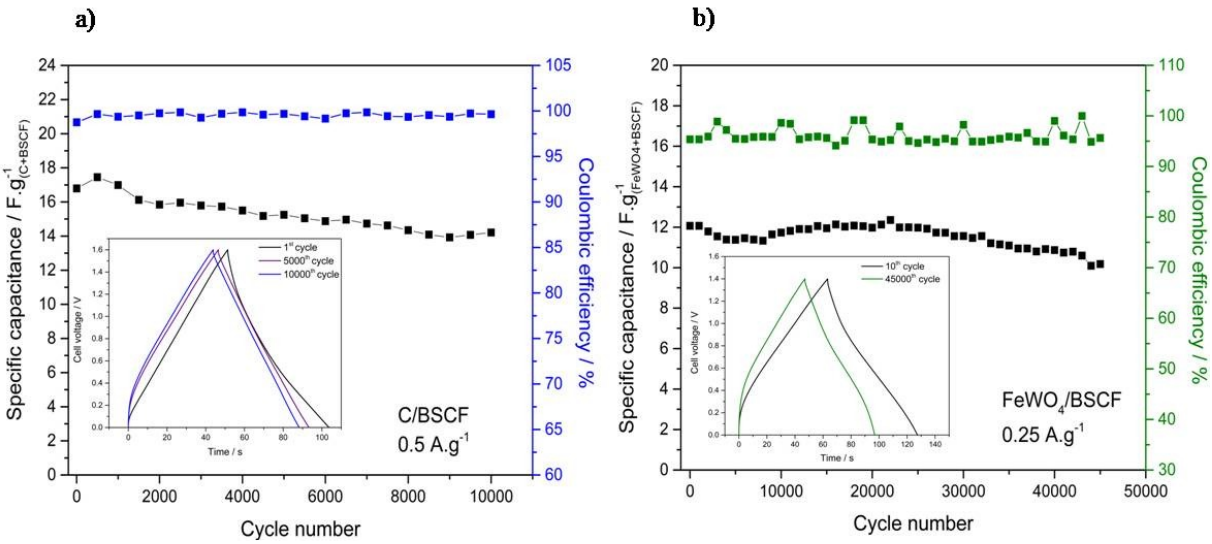

Fig. 5. Cycling ability test performed on a) C/BSCF device with a BSCF/C ratio of 2.1 at 0.5 A.g^{-1} in 5M $LiNO_3$ (evolution of the specific capacitance in black and coulombic efficiency in blue) and b) $FeWO_4$/BSCF device with a BSCF/$FeWO_4$ weight ratio of 2 at 0.25 A.g^{-1} in 5M $LiNO_3$ (evolution of the specific capacitance in black and coulombic efficiency in green). Insets are galvanostatic cycles after various cycles; gravimetric values are expressed per total active weights in both electrodes.

Self-discharge behavior has been evaluated for C/BSCF (BSCF/C weight ratio of 2.1) and $FeWO_4$/BSCF ($FeWO_4$/BSCF weight ratio of 2) devices and compared to that of a symmetric C/C device (cell voltage 1.6 V). The activated carbon used for the symmetric device is the same as for the C/BSCF device. C/C, C/BSCF and $FeWO_4$/BSCF cells have been fully charged to their respective maximum cell voltage, *i.e.* from 0 to 1.6 V, 1.6 V and 1.4 V,

respectively. The corresponding total charges stored Q_{max} are 252, 67 and 44 mC, respectively. The self-discharge profile (plot *vs* the time) measured after a 3 hours polarization at maximum cell voltage is shown in **Fig. 6**. Half of the cell voltage (*i.e.* when half of totals charges stored are released) was reached in 10 and 47 hours respectively for the C/BSCF and $FeWO_4$/BSCF devices. Self-discharge currents of C/BSCF and $FeWO_4$/BSCF are 9 and 4 $\mu A.F^{-1}$, respectively (calculations to determine self-discharge current are described in SI). This is respectively 6 and 14 times lower than the self-discharge current of the C/C device which is 57 $\mu A.F^{-1}$ (with half of the cell voltage reached in only 4 hours). Despite a lower cycling ability, asymmetric C/BSCF and $FeWO_4$/BSCF devices demonstrate improved self-discharge characteristics compared to the symmetric C/C device. A detailed analysis of the self-discharge profiles is provided in SI (**Fig. S10** and **Tab. S6**).

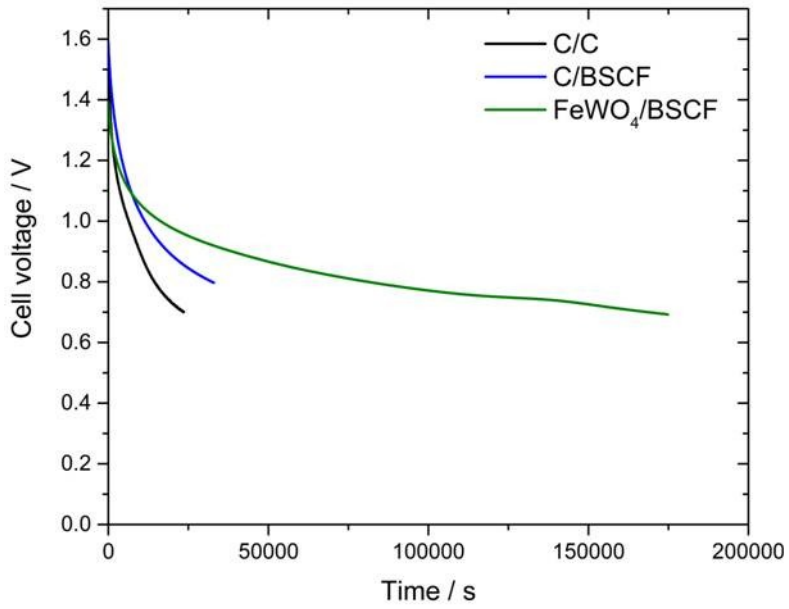

Fig. 6. Self-discharge profile of C/C, C/BSCF and $FeWO_4$/BSCF devices.

4. Conclusion

We report for the first time, two asymmetric electrochemical capacitors based on BSCF positive electrode material. The first one includes an activated carbon based negative

electrode. The second, a $FeWO_4$-based negative electrode, leading to a device with two high density multicationic oxides as electrode materials. The high densities of both oxides, together with the low capacitances of the electrodes led to lower specific performance than those of a symmetrical C/C device. However, the high densities of BSCF and $FeWO_4$ enable electrodes of smaller volume. On one hand, the small volume of electrodes was not sufficient to compensate the limited capacitance of the $FeWO_4$/BSCF device. On the other hand, the high density of BSCF, associated to the high capacitance of activated carbon electrode led to similar volumetric energy density as for the C/C devices, despite a limited capacitance. At low current density (0.2-0.4 $A.g^{-1}$), the C/BSCF device volumetric energy density was even greater than that of the C/C device, at 2.3 $Wh.L^{-1}$ (relative to the volume of electrodes and current collectors). Furthermore, both devices presented attractive cycling abilities upon cycling with a capacitance retention of 88% over 10,000 cycles for the C/BSCF device and 83% over 45,000 cycles for the $FeWO_4$/BSCF device. It is important to notice that such a long cycling test of an asymmetric device built on two pseudocapacitive oxides is scarce in the literature. Furthermore, asymmetric devices present better self-discharge characteristics than the C/C device. Asymmetric devices built on two pseudocapacitive multicationic oxides could be an attractive strategy to improve the volumetric energy density of electrochemical capacitors. However, in aqueous based electrolytes, large specific capacitances are mandatory to compete with symmetric C/C devices, at least 100 $F.g^{-1}$.

Acknowledgements

This work was supported by the French National Agency through IVEDS project - Improving the Volumetric Energy Density of Supercapacitors – ref ANR-15-CE05-0011.

Notes

The authors declare no competing financial interest

References

1 Conway, B. E. Electrochemical Supercapacitors: Scientific Fundamentals and Technological Applications. *Kluwer Academic/Plenum Publishers* (1999).
2 Long, J. W. *et al.* Asymmetric electrochemical capacitors—Stretching the limits of aqueous electrolytes. *MRS Bulletin* **36**, 513-522 (2011).
3 Brousse, T., Bélanger, D. & Long, J. W. To Be or Not To Be Pseudocapacitive? *Journal of The Electrochemical Society* **162**, A5185-A5189 (2015).
4 Trasatti, S. & Buzzanca, G. Ruthenium dioxide: A new interesting electrode material. Solid state structure and electrochemical behaviour. *Journal of Electroanalytical Chemistry and Interfacial Electrochemistry* **29**, A1-A5 (1971).
5 Zheng, J. P., Cygan, P. J. & Jow, T. R. Hydrous Ruthenium Oxide as an Electrode Material for Electrochemical Capacitors. *Journal of The Electrochemical Society* **142**, 2699-2703 (1995).
6 Hu, C.-C., Chen, W.-C. & Chang , K.-H. How to Achieve Maximum Utilization of Hydrous Ruthenium Oxide for Supercapacitors. *Journal of The Electrochemical Society* **151**, A281-A290 (2004).
7 Lee, H. Y. & Goodenough, J. B. Supercapacitor Behavior with KCl Electrolyte. *Journal of Solid State Chemistry* **144**, 220-223 (1999).
8 Toupin, M., Brousse, T. & Bélanger, D. Charge Storage Mechanism of MnO_2 Electrode Used in Aqueous Electrochemical Capacitor. *Chemistry of Materials* **16**, 3184-3190 (2004).
9 Ghodbane, O., Pascal, J.-L. & Favier, F. Microstructural Effects on Charge-Storage Properties in MnO_2-Based Electrochemical Supercapacitors. *ACS Applied Materials & Interfaces* **1**, 1130-1139 (2009).
10 Cottineau, T., Toupin, M., Delahaye, T., Brousse, T. & Bélanger, D. Nanostructured transition metal oxides for aqueous hybrid electrochemical supercapacitors. *Applied Physics A* **82**, 599-606 (2006).
11 Wu, N.-L., Wang, S.-Y., Han, C.-Y., Wu, D.-S. & Shiue, L.-R. Electrochemical capacitor of magnetite in aqueous electrolytes. *Journal of Power Sources* **113**, 173-178 (2003).

12 Choi, D., Blomgren, G. E. & Kumta, P. N. Fast and Reversible Surface Redox Reaction in Nanocrystalline Vanadium Nitride Supercapacitors. *Advanced Materials* **18**, 1178-1182 (2006).
13 Lucio-Porto, R. *et al.* VN thin films as electrode materials for electrochemical capacitors. *Electrochimica Acta* **141**, 203-211 (2014).
14 Liu, T. C., Pell, W. G., Conway, B. E. & Roberson, S. L. Behavior of Molybdenum Nitrides as Materials for Electrochemical Capacitors: Comparison with Ruthenium Oxide. *Journal of The Electrochemical Society* **145**, 1882-1888 (1998).
15 Shown, I., Ganguly, A., Chen, L.-C. & Chen, K.-H. Conducting polymer-based flexible supercapacitor. *Energy Science & Engineering* **3**, 2-26 (2015).
16 Boota, M. *et al.* Pseudocapacitive Electrodes Produced by Oxidant-Free Polymerization of Pyrrole between the Layers of 2D Titanium Carbide (MXene). *Advanced Materials* **28**, 1517-1522 (2016).
17 Goubard-Bretesché, N., Crosnier, O., Favier, F. & Brousse, T. Improving the Volumetric Energy Density of Supercapacitors. *Electrochimica Acta* **206**, 458-463 (2016).
18 Crosnier, O. *et al.* Polycationic oxides as potential electrode materials for aqueous-based electrochemical capacitors. *Current Opinion in Electrochemistry* **9**, 87-94 (2018).
19 Mefford, J. T., Hardin, W. G., Dai, S., Johnston, K. P. & Stevenson, K. J. Anion charge storage through oxygen intercalation in $LaMnO_3$ perovskite pseudocapacitor electrodes. *Nature Materials* **13**, 726 (2014).
20 Hwang, D. K., Kim, S., Lee, J.-H., Hwang, I.-S. & Kim, I.-D. Phase evolution of perovskite $LaNiO_3$ nanofibers for supercapacitor application and p-type gas sensing properties of LaOCl–NiO composite nanofibers. *Journal of Materials Chemistry* **21**, 1959-1965 (2011).
21 Cao, Y., Lin, B., Sun, Y., Yang, H. & Zhang, X. Symmetric/Asymmetric Supercapacitor Based on the Perovskite-type Lanthanum Cobaltate Nanofibers with Sr-substitution. *Electrochimica Acta* **178**, 398-406 (2015).
22 Lü, J. *et al.* A preliminary study of the pseudo-capacitance features of strontium doped lanthanum manganite. *RSC Advances* **5**, 5858-5862 (2015).
23 Cao, Y., Lin, B., Sun, Y., Yang, H. & Zhang, X. Sr-doped Lanthanum Nickelate Nanofibers for High Energy Density Supercapacitors. *Electrochimica Acta* **174**, 41-50 (2015).
24 Abdollahifar, M. *et al.* High-performance carbon-coated $ZnMn_2O_4$ nanocrystallite supercapacitors with tailored microstructures enabled by a novel solution combustion method. *Journal of Power Sources* **378**, 90-97 (2018).
25 Kuo, S.-L., Lee, J.-F. & Wu, N.-L. Study on Pseudocapacitance Mechanism of Aqueous $MnFe_2O_4$ Supercapacitor. *Journal of The Electrochemical Society* **154**, A34-A38 (2007).
26 Kuo, S.-L. & Wu, N.-L. Electrochemical characterization on $MnFe_2O_4$/carbon black composite aqueous supercapacitors. *Journal of Power Sources* **162**, 1437-1443 (2006).
27 Chang, S.-K. *et al.* Structural and electrochemical properties of manganese substituted nickel cobaltite for supercapacitor application. *Electrochimica Acta* **67**, 67-72 (2012).
28 Goubard-Bretesché, N., Crosnier, O., Payen, C., Favier, F. & Brousse, T. Nanocrystalline $FeWO_4$ as a pseudocapacitive electrode material for high volumetric energy density supercapacitors operated in an aqueous electrolyte. *Electrochemistry Communications* **57**, 61-64 (2015).

29 Shanmugavani, A., Murugeswari, R., Sanjeeviraja, C. & Selvan, R. K. Nanocrystalline Pyrochlore $La_2Sn_{1.6}Zr_{0.4}O_7$ as a New Candidate for Supercapacitor Electrodes. *Journal of Nanoscience and Nanotechnology* **15**, 2790-2797 (2015).
30 Lannelongue, P. *et al.* Investigation of $Ba_{0.5}Sr_{0.5}Co_xFe_{1-x}O_{3-\delta}$ as a pseudocapacitive electrode material with high volumetric capacitance. *Electrochimica Acta* **271**, 677-684 (2018).
31 Goubard-Bretesché, N., Crosnier, O., Buvat, G., Favier, F. & Brousse, T. Electrochemical study of aqueous asymmetric $FeWO_4/MnO_2$ supercapacitor. *Journal of Power Sources* **326**, 695-701 (2016).
32 Liu, P. *et al.* $Ba_{0.5}Sr_{0.5}Co_{0.8}Fe_{0.2}O_{3-\delta}$-based dual-gradient cathodes for solid oxide fuel cells. *Ceramics International* **44**, 4516-4519 (2018).
33 Cheng, X., Fabbri, E., Kim, B., Nachtegaal, M. & Schmidt, T. J. Effect of ball milling on the electrocatalytic activity of $Ba_{0.5}Sr_{0.5}Co_{0.8}Fe_{0.2}O_3$ towards the oxygen evolution reaction. *Journal of Materials Chemistry A* **5**, 13130-13137 (2017).
34 Habiballah, A. S., Jani, A. M. M., Mahmud, A. H., Osman, N. & Radiman, S. Facile synthesis of $Ba_{0.5}Sr_{0.5}Co_{0.8}Fe_{0.2}O_{3-\delta}$ (BSCF) perovskite nanowires by templating from nanoporous anodic aluminium oxide membranes. *Materials Chemistry and Physics* **177**, 371-378 (2016).
35 Tan, L. A. *et al.* Influence of powder synthesis methods on microstructure and oxygen permeation performance of $Ba_{0.5}Sr_{0.5}Co_{0.8}Fe_{0.2}O_{3-\delta}$ perovskite-type membranes. *Journal of Membrane Science* **212**, 157-165 (2003).
36 Wang, H. H., Tablet, C., Feldhoff, A. & Caro, H. Investigation of phase structure, sintering, and permeability of perovskite-type $Ba_{0.5}Sr_{0.5}Co_{0.8}Fe_{0.2}O_{3-\delta}$ membranes. *Journal of Membrane Science* **262**, 20-26 (2005).
37 Kovács, T. N. *et al.* Preparation of iron tungstate ($FeWO_4$) nanosheets by hydrothermal method. *Materials Research Bulletin* **95**, 563-569 (2017).
38 Niu, L. *et al.* Simple Synthesis of Amorphous $NiWO_4$ Nanostructure and Its Application as a Novel Cathode Material for Asymmetric Supercapacitors. *ACS Applied Materials & Interfaces* **5**, 8044-8052 (2013).
39 Balducci, A., Belanger, D., Brousse, T., Long, J. W. & Sugimoto, W. Perspective—A Guideline for Reporting Performance Metrics with Electrochemical Capacitors: From Electrode Materials to Full Devices. *Journal of The Electrochemical Society* **164**, A1487-A1488 (2017).
40 Soeda, K., Yamagata, M. & Ishikawa, M. Outstanding features of alginate-based gel electrolyte with ionic liquid for electric double layer capacitors. *Journal of Power Sources* **280**, 565-572 (2015).
41 Liu, Y. & Zhitomirsky, I. Electrochemical supercapacitor based on multiferroic $BiMn_2O_5$. *Journal of Power Sources* **284**, 377-382 (2015).
42 Brousse, T. *et al.* Long-term cycling behavior of asymmetric activated carbon/MnO_2 aqueous electrochemical supercapacitor. *Journal of Power Sources* **173**, 633-641 (2007).
43 Raut, S. S. *et al.* Zinc Ferrite Anchored Multiwalled Carbon Nanotubes for High-Performance Supercapacitor Applications. *European Journal of Inorganic Chemistry* **2018**, 137-142 (2018).
44 Su, Y. & Zhitomirsky, I. Hybrid MnO_2/carbon nanotube-VN/carbon nanotube supercapacitors. *Journal of Power Sources* **267**, 235-242 (2014).
45 Brousse, T. & Bélanger, D. A Hybrid Fe_3O_4 /MnO_2 Capacitor in Mild Aqueous Electrolyte. *Electrochemical and Solid-State Letters* **6**, A244-A248 (2003).